Periosteal response to bone fracture at single nuclei resolution

Simon Perrin[1], Cécile-Aurore Wotawa[1], Marine Luka[2,3], Fanny Coulpier[1], Cécile Masson[4,5], Mickael Ménager[2,3], and Céline Colnot[1]

[1] Univ Paris Est Creteil, INSERM, IMRB, Creteil, France

[2]Paris Cité University, Imagine Institute, Laboratory of Inflammatory Responses and Transcriptomic Networks in Diseases, Atip-Avenir Team, INSERM UMR 1163, Paris, France.

[3] Labtech Single-Cell@Imagine, Imagine Institute, INSERM UMR 1163, Paris, France.

[4] Bioinformatics Core Facility, Institut Imagine-Structure Fédérative de Recherche Necker, INSERM U1163

[5] INSERM US24/CNRS UAR3633, Paris Cité University, Paris, France

Summary

Bone regeneration is a highly efficient process allowing bones to fully regenerate after fracture. Skeletal stem/progenitor cells (SSPCs) allowing bone regeneration are recruited from several sources, including the periosteum located at the outer surface of bones. Periosteal SSPCs are major actors of bone healing and display the unique property to form both bone and cartilage after fracture. Yet, the steps of periosteal SSPCs activation and differentiation leading to osteogenesis and chondrogenesis remain poorly understood. Here, we generated a single-nuclei atlas of the periosteum at steady-state and in response to bone fracture. We described the heterogeneity of the uninjured periosteum and identified a population of periosteal SSPCs expressing stemness markers, such as *Pi16* and *Ly6a* (Sca1). After fracture, we observed major changes in cell populations with a reduction of the SSPC population, a concomitant increase in injury-induced fibrogenic cells and immune cells, followed by the appearance of chondrocytes and osteoblasts. We show that periosteal SPPCs respond to injury via a unique differentiation trajectory. Cells first leave their stem/progenitor state to adopt an injury-activated fibrogenic fate, prior to undergoing either osteogenesis or chondrogenesis. Overall, our study provides a complete temporal topography of the fracture healing environment and the dynamic response of periosteal SSPC to injury, redefining our knowledge on the early steps of bone regeneration.

Keywords

periosteum – bone repair – skeletal stem/progenitor cells – single nuclei RNAseq

Introduction

The skeleton provides structural support and protection for internal organs in the vertebrate body. Continuously solicited, bones can fracture, but regenerate themselves efficiently without scarring. Bone regeneration is mediated by the action of resident skeletal stem/progenitor cells (SSPCs) from bone marrow and periosteum and also from the skeletal muscle adjacent to the fracture site (Debnath et al., 2018; Duchamp de Lageneste et al., 2018; Jeffery et al., 2022; Julien et al., 2022, 2021). SSPCs become activated during the inflammatory phase of healing and differentiate into osteoblasts and/or chondrocytes. These SSPCs can participate in bone regeneration via a combination of endochondral and intramembranous ossification. During intramembranous ossification SSPCs differentiate directly into osteoblasts, while during endochondral ossification SSPCs first differentiate into chondrocytes to form an intermediate cartilage template subsequently replaced by bone.

The periosteum, an heterogenous tissue on the outer surface of bones, is a crucial source of SSPCs during bone healing (Debnath et al., 2018; Duchamp de Lageneste et al., 2018; Jeffery et al., 2022; Matthews et al., 2021). Periosteal SSPCs exhibit a high regenerative potential. They also display a unique osteochondrogenic potential after injury compared to cells from the bone marrow that are mostly osteogenic and cells from skeletal muscle that are mostly chondrogenic (Duchamp de Lageneste et al., 2018; Jeffery et al., 2022; Julien et al., 2022, 2021; Matsushita et al., 2020). Periosteal SSPCs (pSSPCs) are still poorly characterized, their bipotentiality and response to bone injury also remain elusive. Recent advances in single cell/nuclei transcriptomic analyses provided new insights in stem cell population heterogeneity and regeneration processes in many organs (De Micheli et al., 2020; Guerrero-Juarez et al., 2019; Storer et al., 2020). However, few studies have investigated bone healing at the single cell level and these studies have focused on cultured cells or late stages of bone repair (Julien et al., 2022; Sivaraj et al., 2022). A complete dataset of periosteum and bone regeneration to decipher the mechanisms of pSSPC activation and regulation is lacking. Here, we created a

single-nuclei atlas of the periosteum and its response to bone fracture. We generated single nuclei RNAseq (snRNAseq) datasets from the uninjured periosteum and from the periosteum and hematoma/callus at days 3, 5 and 7 post-tibial fracture. Our analyses thoroughly describe the heterogeneity of the periosteum at steady state and the steps of pSSPC activation after injury. We show that pSSPC represent a unique SSPC population that can provide osteoblasts and chondrocytes for bone repair by first generating a common injury-induced fibrogenic cell population that engage into osteogenesis or chondrogenesis.

Results

Heterogeneity of the periosteum at steady state

To investigate the heterogeneity of the periosteum at steady-state, we performed snRNAseq of the periosteum of wild-type mice (Fig. 1A-B). After filtering, we obtained 1189 nuclei, corresponding to 7 cell populations: SSPC/fibroblasts (expressing *Pdgfra*), osteogenic cells (expressing *Runx2*), Schwann cells (expressing *Mpz*) pericytes/SMC (expressing *Tagln*), immune cells (expressing *Ptprc*), adipocytes (expressing *Lpl*), and endothelial cells (ECs, expressing *Pecam1*) (Fig. 1C-D). The EC population was divided into arteriolar ECs (expressing *Sox17*), veinous ECs (expressing *Vwf*), capillary ECs (expressing *Rgcc*) and lymphatic ECs (expressing *Mmrn1*) (Fig. S1). We performed in depth analyses of the SSPC/fibroblast and osteogenic cell populations. Subset analyses of clusters 0, 1, 2, 3, 4 and 5 identified 5 distinct SSPC/fibroblast cell populations expressing *Pdgfra* and *Prrx1*: *Ly6a*$^{+}$ (Sca1^{+}), *Hmcn2*$^{+}$*, Hsd11b1*$^{+}$*, Cldn1*$^{+}$*,* and *Luzp2*$^{+}$cells (Fig. 1E-G). Sca1+ cells (i.e. cluster 0) were the only cluster expressing stemness markers including *Pi16, Dpp4,* and *Cd34* (Fig. 1H). Cytotrace scoring identified Sca1+ cells as the population in the most undifferentiated state, suggesting that this population corresponds to periosteal SSPCs (Fig. 1I). We explored the expression of other known markers of periosteal SSPCs, including *Ctsk*, *Acta2* (αSMA), and *Mx1*, but no marker was fully specific to one cell cluster (Fig. S2).

The fracture repair atlas

To investigate the periosteal response to bone fracture, we collected injured periosteum with hematoma or calluses at days 3, 5 and 7 post-fracture, extracted the nuclei and processed them for snRNAseq (Fig. 2A). We combined the datasets with the uninjured periosteum from Figure 1 and obtained a total of 6213 nuclei. The combined dataset was composed of 26 clusters corresponding to 10 cell populations: SSPCs (expressing *Pi16*), injury-induced fibrogenic cells (IIFC, expressing *Postn*), osteoblasts (expressing *Ibsp*), chondrocytes (expressing *Col2a1*), osteoclasts (expressing *Ctsk*), immune cells (expressing *Ptprc*), Schwann cells (expressing *Mpz*), endothelial cells (expressing *Pecam1*), pericyte/SMC (expressing *Pdgfrb*), and adipocytes

(expressing *Lpl*) (Fig. 2B-C, Fig. S2A). Next, we observed the dynamics of the cell populations in response to bone fracture (Fig. 2D, Fig. S2B). The percentage of SSPCs was strongly decreased and the percentage of IIFCs progressively increased after injury (Fig. 2E). The percentage of chondrocytes and osteoblasts increased from day 3 post-fracture. Immune cells were drastically increased at day 3 after injury, before progressively decreasing at days 5 and 7 post-fracture (Fig. 2E).

Periosteal SSPCs differentiate through a common injury-induced fibrogenic stage.

To understand the differentiation and fate of pSSPCs after fracture, we analyzed the subset of SSPC, IIFC, chondrocyte and osteoblast clusters from the combined fracture dataset (Fig. 3A). We performed pseudotime analysis to determine the differentiation trajectories, defining the starting point in the SSPC population, where the uninjured and undifferentiated cells clustered. We identified that SSPC response to fracture progresses in 3 stages starting from the SSPC population (expressing *Ly6a*, *Cd34* and *Dpp4*), predominant in uninjured dataset (Fig. 3B-E). Periosteal SSPCs then transition through a common injury-induced fibrogenic stage predominant at days 3 and 5 post-injury. Cells in this intermediate fibrogenic stage express high levels of extracellular matrix genes, such as *Postn*, *Aspn* and *Tnc*. Finally, injury-induced fibrogenic cells differentiate into chondrocytes (expressing *Acan*, *Col2a1* and *Sox9*) or osteoblasts (expressing *Sp7*, *Alpl* and *Ibsp*), both predominant at days 5 and 7 (Fig. 3B-E). These results show that pSSPC undergo a unique activation trajectory, independent of their final fate (Fig. 3F).

Discussion

The periosteum is the main driver of bone regeneration, yet the periosteum response to bone fracture is poorly described. Here, we used single-nuclei transcriptomics to understand the heterogeneity of the periosteum at steady state and the changes occurring within periosteum after bone fracture. We developed a protocol to extract nuclei from freshly dissected periosteum, allowing to capture their intact transcriptomic profile without enzymatic digestion-induced stress (Ding et al., 2020; Machado et al., 2021; van den Brink et al., 2017). In addition, we performed snRNAseq without sorting specific populations, allowing the identification of all cell types located in the periosteum and the fracture environment from the early stages of repair. Our study provides the first complete fracture repair atlas, a key tool to understand bone regeneration.

First, we described the heterogeneity of the periosteum at steady state. While previous studies performed scRNAseq on sorted periosteal cell populations, our dataset demonstrate the diversity of cell populations within the periosteum. We identified 5 fibroblast populations, as well as blood vessel and nerve-related cells. Among the fibroblast population, we identified one SSPC population of undifferentiated cells expressing markers such as Sca1 and *Pi16,* known to mark fibroblasts with stemness potential (Buechler et al., 2021). No markers previously described such as *Ctsk*, or *Gli1* were fully specific of one cell cluster, suggesting that these markers may label heterogenous cell populations (Debnath et al., 2018; Jeffery et al., 2022; Matthews et al., 2021).

After fracture, the composition of the periosteum changes drastically, with the appearance of IIFC and immune cells from day 3 post-fracture, and of chondrocytes and osteoblasts from day 5 post-fracture. Previous studies based on in vitro analyses and in vivo lineage tracing demonstrated that the periosteum displays the unique potential to form both bone and cartilage after fracture (Debnath et al., 2018; Duchamp de Lageneste et al., 2018; Julien et al., 2022). Yet, it was still unknown if the periosteum contains a bipotent SSPC population or several SSPC populations with distinct potentials after injury. Here, we show that pSSPCs activate and form bone and cartilage via a unique trajectory emerging from Sca1+ SSPCs. Periosteal Sca1+ SSPCs become IIFCs, a state marked by a decreased expression of stemness markers and a strong expression of extracellular matrix genes, such as *Postn* and *Aspn*. Following this unique fibrogenic step, IIFC undergo either osteogenesis or chondrogenesis. This newly identified transient IIFC state represents the crossroad of bone regeneration and SSPC differentiation. In depth analyses of the IIFC phase and the mechanisms regulating cell fate decision are needed as IIFC might represent the ideal target to enhance bone healing and potentially treat bone repair defects.

Overall, our study provides a complete dataset of the early steps of bone regeneration. Further analyses will establish the mechanisms regulating pSSPCs cell fate decisions and the role other cell populations play in the fracture environment.

Data availability

Single nuclei RNAseq datasets are deposited in the Gene Expression Omnibus (GSE234451).

Acknowledgements

This work was supported by ANR-18-CE14-0033, ANR-21-CE18-007-01and NIAMS R01 AR072707 to C. C. and Ted Miclau. S. Perrin was supported by a PhD fellowship from Paris Cité University. We thank O. Pellé from the Flow Cytometry platform at Imagine Institute and all the staff from the Imagine genomic core facility at Imagine Institute.

Competing interests

Authors declare no competing interests.

Figures

Figure 1

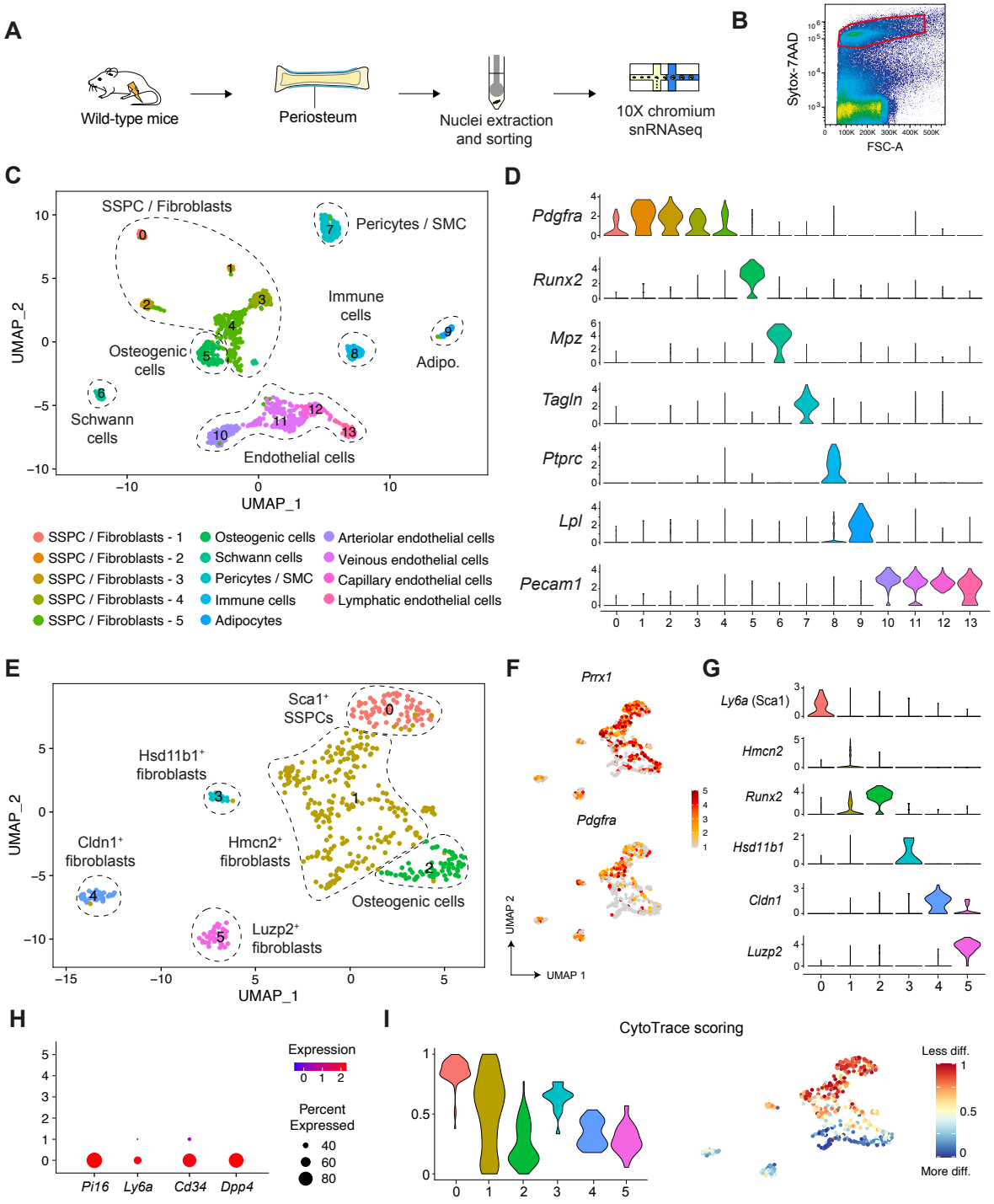

Figure 1: Heterogeneity of the periosteum at steady state

A. Experimental design. Nuclei were extracted from the periosteum of uninjured tibia and processed for single-nuclei RNAseq. **B.** Sorting strategy of nuclei stained with Sytox-7AAD for snRNAseq. Sorted nuclei are delimited by a red box. **C.** UMAP projection of color-coded clustering of the uninjured periosteum dataset. Six populations are identified and delimited by black dashed lines. **D.** Violin plots of key marker genes of the different cell populations. **E.** UMAP projection of color-coded clustering of the subset of SSPC/fibroblasts. **F.** Feature plots of *Prrx1* and *Pdgfra* in the subset of SSPC/fibroblasts. **G.** Feature plots of key marker genes of the different cell populations. **H.** Dot plot of the stemness markers *Pi16, Ly6a* (Sca1*), Cd34,* and *Dpp4*. **G.** Violin and feature plots of Cytotrace scoring in the subset of SSPC/fibroblasts, showing that Sca1+ SSPCs (cluster 0) are the less differentiated cells in the dataset.

Figure 2

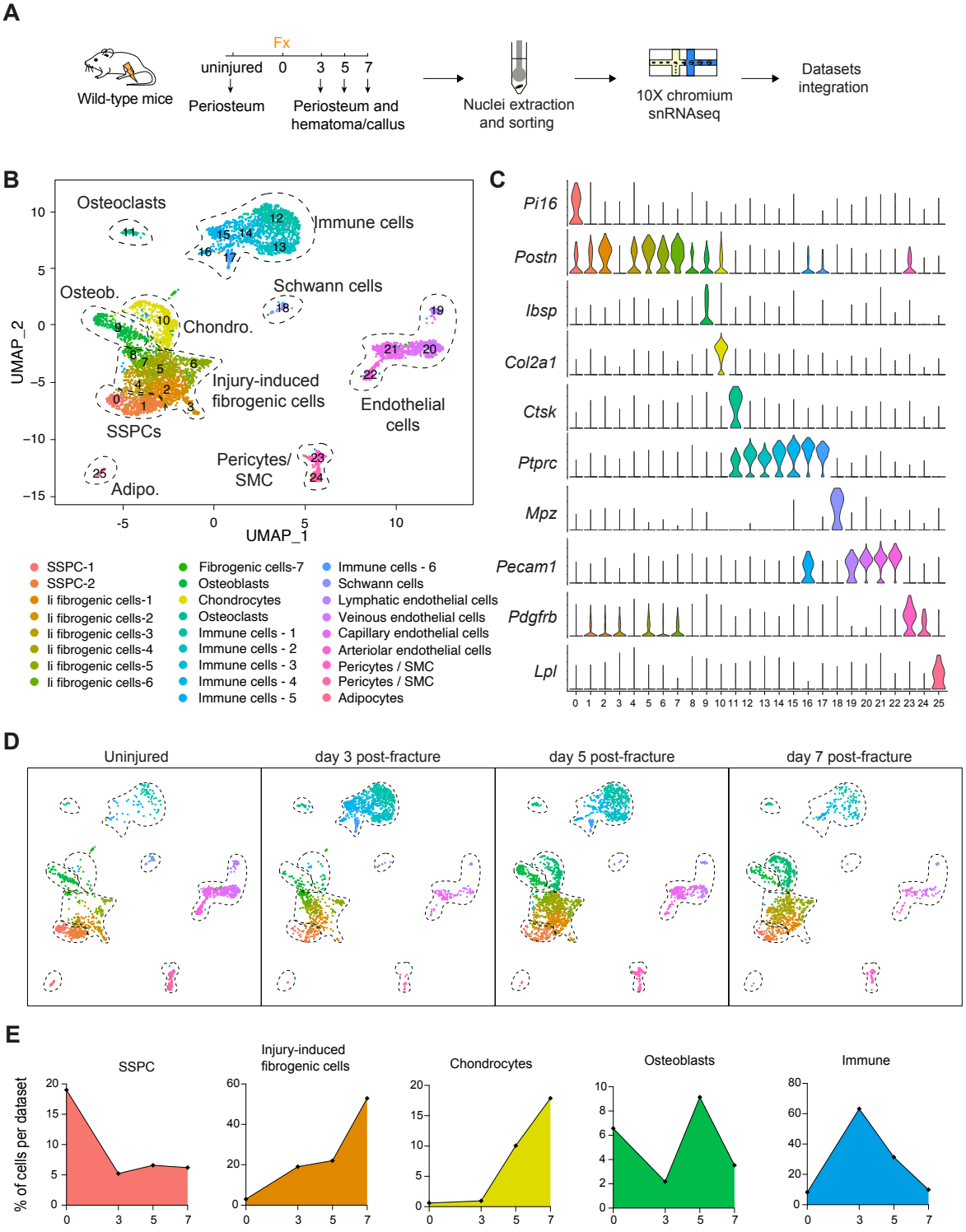
A
Wild-type mice
Fx
uninjured 0 3 5 7
Periosteum
Periosteum and hematoma/callus
Nuclei extraction and sorting
10X chromium snRNAseq
Datasets integration
B
Osteoclasts
Immune cells
Schwann cells
Osteob.
Chondro.
Injury-induced fibrogenic cells
Endothelial cells
SSPCs
Pericytes/ SMC
Adipo.
UMAP_2
UMAP_1
SSPC-1
SSPC-2
li fibrogenic cells-1
li fibrogenic cells-2
li fibrogenic cells-3
li fibrogenic cells-4
li fibrogenic cells-5
li fibrogenic cells-6
Fibrogenic cells-7
Osteoblasts
Chondrocytes
Osteoclasts
Immune cells - 1
Immune cells - 2
Immune cells - 3
Immune cells - 4
Immune cells - 5
Immune cells - 6
Schwann cells
Lymphatic endothelial cells
Veinous endothelial cells
Capillary endothelial cells
Arteriolar endothelial cells
Pericytes / SMC
Pericytes / SMC
Adipocytes
C
Pi16
Postn
Ibsp
Col2a1
Ctsk
Ptprc
Mpz
Pecam1
Pdgfrb
Lpl
D
Uninjured
day 3 post-fracture
day 5 post-fracture
day 7 post-fracture
E
SSPC
Injury-induced fibrogenic cells
Chondrocytes
Osteoblasts
Immune
% of cells per dataset

Figure 2: Periosteal response to fracture at single-nuclei resolution

A. Experimental design. Nuclei were extracted from the periosteum of uninjured tibia of wild-type mice and from the periosteum and hematoma at days 3, 5 and 7 post-tibial fracture and processed for single-nuclei RNAseq. **B.** UMAP projection of color-coded clustering of the integration of uninjured, day 3, day 5 and day 7 datasets. Ten populations are identified and delimited by black dashed lines. **C.** Violin plots of key marker genes of the different cell populations. **D.** UMAP projection of the combined dataset separated by time-point. **E.** Percentage of cells in SSPC, injury-induced fibrogenic cell, osteoblast, chondrocyte, and immune cell clusters in uninjured, day 3, day 5 and day 7 datasets.

Figure 3

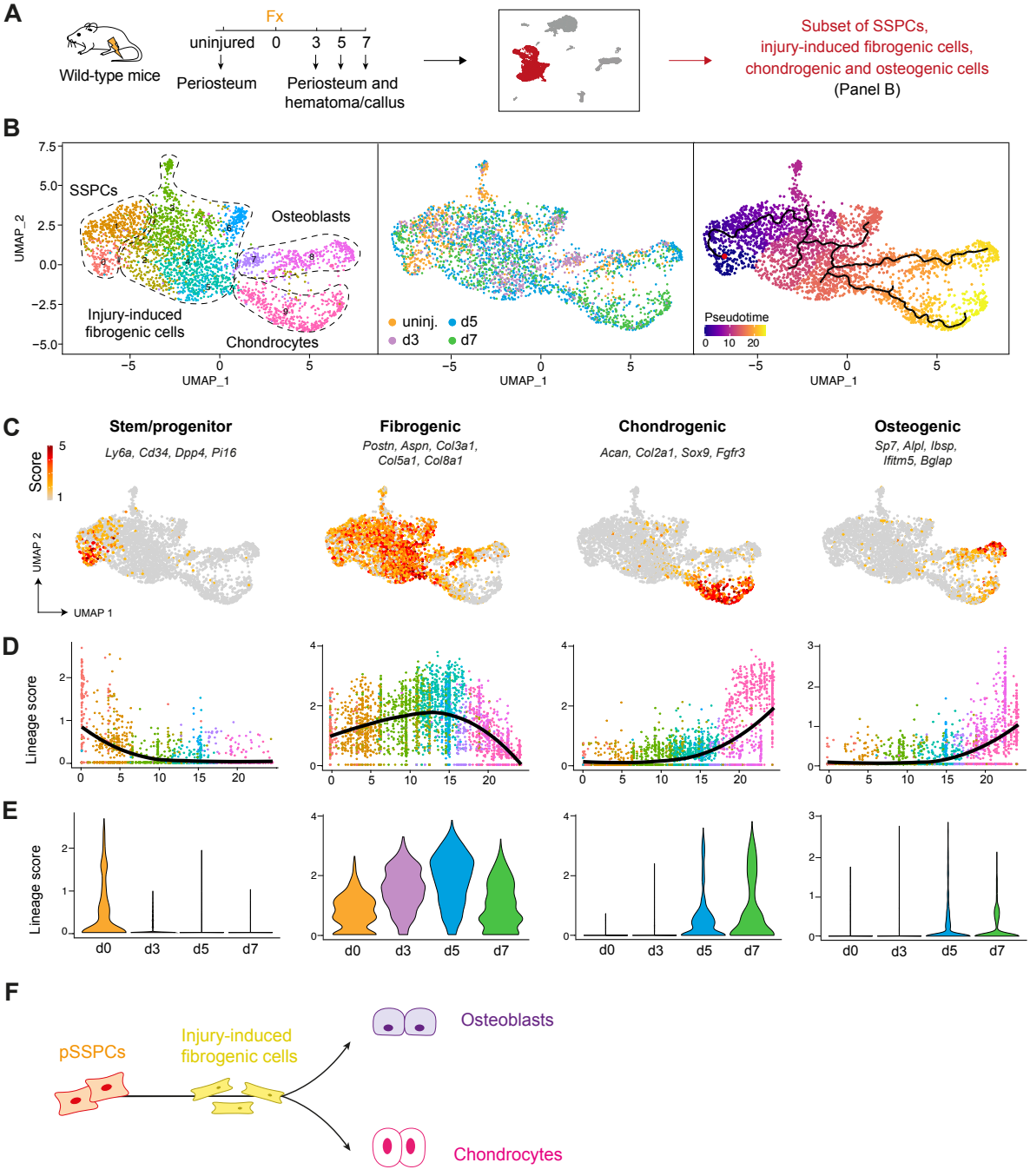
A
Wild-type mice
Fx
uninjured
0
3
5
7
Periosteum
Periosteum and hematoma/callus
Subset of SSPCs, injury-induced fibrogenic cells, chondrogenic and osteogenic cells (Panel B)
B
SSPCs
Osteoblasts
Injury-induced fibrogenic cells
Chondrocytes
UMAP_2
UMAP_1
uninj.
d3
d5
d7
Pseudotime
C
Stem/progenitor
Ly6a, Cd34, Dpp4, Pi16
Fibrogenic
Postn, Aspn, Col3a1, Col5a1, Col8a1
Chondrogenic
Acan, Col2a1, Sox9, Fgfr3
Osteogenic
Sp7, Alpl, Ibsp, Ifitm5, Bglap
Score
UMAP 2
UMAP 1
D
Lineage score
E
Lineage score
d0
d3
d5
d7
F
pSSPCs
Injury-induced fibrogenic cells
Osteoblasts
Chondrocytes

Figure 3: Periosteal SSPCs activate through a common fibrogenic state prior to undergoing osteogenesis or chondrogenesis

A. SSPCs, injury-induced fibrogenic cells (IIFCs), chondrocytes and osteoblasts from integrated uninjured, day 3, day 5 and day 7 post-fracture samples were extracted for a subset analysis. **B.** UMAP projection of color-coded clustering (left), color-coded sampling (middle) and monocle pseudotime trajectory (right) of the subset dataset. The four populations are delimited by black dashed lines. **C.** Feature plots of the lineage scores of the four populations**. D-E.** Feature plot (D) and scatter plot (E) of stem/progenitor, fibrogenic chondrogenic and osteogenic lineage scores along pseudotime in pSSPCs and their derivatives. **F.** Schematic representation of the activation trajectory of pSSPCs after fracture.

Materials and Methods

Mice

C57BL/6ScNj were obtained from Janvier Labs (France). Mice were bred in animal facilities at IMRB, Creteil and kept in separated ventilated cages, in pathogen-controlled environment and ad libitum access to water and food. All procedures performed were approved by Paris Est Creteil University Ethical Committee. Twelve-week-old males and females were mixed in experimental groups.

Tibial fracture

Open non-stabilized tibial fractures were induced as previously described (Perrin et al., 2021). Mice were anesthetized with an intraperitoneal injection of Ketamine (50 mg/mL) and Medetomidine (1 mg/kg) and received a subcutaneous injection of Buprenorphine (0.1 mg/kg) for analgesia. Mice were kept on a 37°C heating pad during anesthesia. The right hindlimb was shaved and sanitized. The skin was incised to expose the tibia and osteotomy was performed in the mid-diaphysis by cutting the bone. The wound was sutured, the mice were revived with an intraperitoneal injection of atipamezole (1 mg/kg) and received two additional analgesic injections in the 24 hours following surgery. Mice were sacrifice 3, 5 or 7 days post-fracture.

Nuclei extraction

Nuclei extraction protocol was adapted from (G Martelotto, 2019; Santos et al., 2021). We generated 4 datasets for this study: uninjured periosteum, periosteum and hematoma at days 3, 5 and 7 post-tibial fracture. The uninjured and day 3 post-fracture datasets were generated in duplicates. For uninjured periosteum, tibias from 4 mice were dissected free of muscle and surrounding tissues. The epiphyses were cut and the bone marrow flushed. The periosteum was scraped from the cortex using dissecting Chisel (10095-12, Fine Science Tools). For days 3, 5 and 7 post fracture, injured tibias from 4 to 9 mice were collected and the surrounded tissues were removed. The activated periosteum was scraped and collected with the hematoma. Collected tissues were minced and placed 5 min in ice-cold Nuclei Buffer (NUC101, Merck) before mechanical nuclei extraction using a glass douncer. Extraction was performed by 20 strokes of pestle A followed by 5-10 of pestle B. Nuclei suspension was filtered, centrifuged and resuspensed in RNAse-free PBS (AM9624, ThermoFischer Scientific) with 2% Bovine Serum Albumin (A2153, Merck) and 0.2 U/µL RNAse inhibitor (3335399001, Roche). A second step of centrifugation

was performed to reduce contamination by cytoplasmic RNA. Sytox™ AADvanced™ (S10349, ThermoFischer Scientific) was added (1/200) to label nuclei and Sytox-AAD+ nuclei were sorted using Sony SH800.

Single nuclei RNA sequencing

The snRNA-seq libraries were generated using Chromium Single Cell Next GEM 3′ Library & Gel Bead Kit v.3.1 (10x Genomics) according to the manufacturer's protocol. Briefly, 10 000 to 20 000 nuclei were loaded in the 10x Chromium Controller to generate single-nuclei gel-beads in emulsion. After reverse transcription, gel-beads in emulsion were disrupted. Barcoded complementary DNA was isolated and amplified by PCR. Following fragmentation, end repair and A-tailing, sample indexes were added during index PCR. The purified libraries were sequenced on a Novaseq (Illumina) with 28 cycles of read 1, 8 cycles of i7 index and 91 cycles of read 2. Sequencing data were processed using the Cell Ranger Count pipeline and reads were mapped on the mm10 reference mouse genome with intronic and exonic sequences.

Filtering and clustering using Seurat

Single-nuclei RNAseq analyses were performed using Seurat v4.1.0 (Butler et al., 2018; Stuart et al., 2019) and Rstudio v1.4.1717. Aligned snRNAseq datasets were filtered to retain only nuclei expressing between 200 et 5000 genes and expressing less than 2% of mitochondrial genes and 1.5% of ribosomal genes. Contamination from myogenic cells were removed from the analyses. After filtering, we obtained 1378 nuclei from uninjured periosteum, 1634 from day 3 post-fracture, 2089 from d5 post-fracture and 1112 from day 7 post-fracture. The replicates of the uninjured dataset were integrated using Seurat. The integrated dataset was regressed on cell cycle, mitochondrial and ribosomal content and clustering was performed using the first 15 principal components and a resolution of 0.5. SSPC/fibroblast and osteogenic cells were isolated and reclustered using the first 10 principal components and a resolution of 0.2. Uninjured, d3, d5 and d7 datasets were integrated using Seurat. The integrated dataset was regressed on cell cycle, mitochondrial and ribosomal content. Clustering was performed using the first 20 principal components and a resolution of 1.3. SSPC, IIFC, chondrogenic and osteogenic clusters from the integration were isolated to perform subset analysis. The subset was reclustered using the first 15 principal components and a resolution of 0.6.

Pseudotime analysis using monocle3

Monocle3 v1.0.0 was used for pseudotime analysis (Cao et al., 2019). Single-cell trajectories were determined using monocle3 default parameters. The starting point of the pseudotime trajectory was determined as the cells from the uninjured dataset with the highest expression of stem/progenitor marker genes *(Ly6a, Cd34, Dpp4, Pi16)*.

Differentiation state analysis using Cytrotrace

To assess the level of differentiation of the cell clusters, we performed analyses using CytoTrace with the default parameters. Cytotrace scoring was plotted in violon plot and on the Seurat UMAP clustering.

References

Buechler, M.B., Pradhan, R.N., Krishnamurty, A.T., Cox, C., Calviello, A.K., Wang, A.W., Yang, Y.A., Tam, L., Caothien, R., Roose-Girma, M., Modrusan, Z., Arron, J.R., Bourgon, R., Müller, S., Turley, S.J., 2021. Cross-tissue organization of the fibroblast lineage. Nature 593, 575–579. https://doi.org/10.1038/s41586-021-03549-5

Butler, A., Hoffman, P., Smibert, P., Papalexi, E., Satija, R., 2018. Integrating single-cell transcriptomic data across different conditions, technologies, and species. Nat Biotechnol 36, 411–420. https://doi.org/10.1038/nbt.4096

Cao, J., Spielmann, M., Qiu, X., Huang, X., Ibrahim, D.M., Hill, A.J., Zhang, F., Mundlos, S., Christiansen, L., Steemers, F.J., Trapnell, C., Shendure, J., 2019. The single-cell transcriptional landscape of mammalian organogenesis. Nature 566, 496–502. https://doi.org/10.1038/s41586-019-0969-x

De Micheli, A.J., Laurilliard, E.J., Heinke, C.L., Ravichandran, H., Fraczek, P., Soueid-Baumgarten, S., De Vlaminck, I., Elemento, O., Cosgrove, B.D., 2020. Single-Cell Analysis of the Muscle Stem Cell Hierarchy Identifies Heterotypic Communication Signals Involved in Skeletal Muscle Regeneration. Cell Rep 30, 3583-3595.e5. https://doi.org/10.1016/j.celrep.2020.02.067

Debnath, S., Yallowitz, A.R., McCormick, J., Lalani, S., Zhang, T., Xu, R., Li, N., Liu, Y., Yang, Y.S., Eiseman, M., Shim, J.-H., Hameed, M., Healey, J.H., Bostrom, M.P., Landau, D.A., Greenblatt, M.B., 2018. Discovery of a periosteal stem cell mediating intramembranous bone formation. Nature 562, 133–139. https://doi.org/10.1038/s41586-018-0554-8

Ding, J., Adiconis, X., Simmons, S.K., Kowalczyk, M.S., Hession, C.C., Marjanovic, N.D., Hughes, T.K., Wadsworth, M.H., Burks, T., Nguyen, L.T., Kwon, J.Y.H., Barak, B., Ge, W., Kedaigle, A.J., Carroll, S., Li, S., Hacohen, N., Rozenblatt-Rosen, O., Shalek, A.K., Villani, A.-C., Regev, A., Levin, J.Z., 2020. Systematic comparison of single-cell and single-nucleus RNA-sequencing methods. Nat Biotechnol 38, 737–746. https://doi.org/10.1038/s41587-020-0465-8

Duchamp de Lageneste, O., Julien, A., Abou-Khalil, R., Frangi, G., Carvalho, C., Cagnard, N., Cordier, C., Conway, S.J., Colnot, C., 2018. Periosteum contains skeletal stem cells with high bone regenerative potential controlled by Periostin. Nat Commun 9, 773. https://doi.org/10.1038/s41467-018-03124-z

G Martelotto, L., 2019. ‘Frankenstein’ protocol for nuclei isolation from fresh and frozen tissue for snRNAseq v2 (preprint). https://doi.org/10.17504/protocols.io.3fkgjkw

Guerrero-Juarez, C.F., Dedhia, P.H., Jin, S., Ruiz-Vega, R., Ma, D., Liu, Y., Yamaga, K., Shestova, O., Gay, D.L., Yang, Z., Kessenbrock, K., Nie, Q., Pear, W.S., Cotsarelis, G., Plikus, M.V., 2019. Single-cell analysis reveals fibroblast heterogeneity and myeloid-derived adipocyte progenitors in murine skin wounds. Nat Commun 10, 650. https://doi.org/10.1038/s41467-018-08247-x

Jeffery, E.C., Mann, T.L.A., Pool, J.A., Zhao, Z., Morrison, S.J., 2022. Bone marrow and periosteal skeletal stem/progenitor cells make distinct contributions to bone maintenance and repair. Cell Stem Cell 29, 1547-1561.e6. https://doi.org/10.1016/j.stem.2022.10.002

Julien, A., Kanagalingam, A., Martínez-Sarrà, E., Megret, J., Luka, M., Ménager, M., Relaix, F., Colnot, C., 2021. Direct contribution of skeletal muscle mesenchymal progenitors to bone repair. Nature Communications 12, 2860. https://doi.org/10.1038/s41467-021-22842-5

Julien, A., Perrin, S., Martínez-Sarrà, E., Kanagalingam, A., Carvalho, C., Luka, M., Ménager, M., Colnot, C., 2022. Skeletal stem/progenitor cells in periosteum and skeletal muscle share a common molecular response to bone injury. J of Bone & Mineral Res jbmr.4616. https://doi.org/10.1002/jbmr.4616

Machado, L., Geara, P., Camps, J., Dos Santos, M., Teixeira-Clerc, F., Van Herck, J., Varet, H., Legendre, R., Pawlotsky, J.-M., Sampaolesi, M., Voet, T., Maire, P., Relaix, F., Mourikis, P., 2021. Tissue damage induces a conserved stress response that initiates quiescent muscle stem cell activation. Cell Stem Cell 28, 1125-1135.e7. https://doi.org/10.1016/j.stem.2021.01.017

Matsushita, Y., Nagata, M., Kozloff, K.M., Welch, J.D., Mizuhashi, K., Tokavanich, N., Hallett, S.A., Link, D.C., Nagasawa, T., Ono, W., Ono, N., 2020. A Wnt-mediated transformation of the bone marrow stromal cell identity orchestrates skeletal regeneration. Nat Commun 11, 332. https://doi.org/10.1038/s41467-019-14029-w

Matthews, B.G., Novak, S., Sbrana, F.V., Funnell, J.L., Cao, Y., Buckels, E.J., Grcevic, D., Kalajzic, I., 2021. Heterogeneity of murine periosteum progenitors involved in fracture healing. eLife 10, e58534. https://doi.org/10.7554/eLife.58534

Perrin, S., Julien, A., Duchamp de Lageneste, O., Abou-Khalil, R., Colnot, C., 2021. Mouse Periosteal Cell Culture, in vitro Differentiation, and in vivo Transplantation in Tibial Fractures. BIO-PROTOCOL 11. https://doi.org/10.21769/BioProtoc.4107

Santos, M.D., Gioftsidi, S., Backer, S., Machado, L., Relaix, F., Maire, P., Mourikis, P., 2021. Extraction and sequencing of single nuclei from murine skeletal muscles. STAR Protocols 2, 100694.

https://doi.org/10.1016/j.xpro.2021.100694

Sivaraj, K.K., Majev, P.-G., Jeong, H.-W., Dharmalingam, B., Zeuschner, D., Schröder, S., Bixel, M.G., Timmen, M., Stange, R., Adams, R.H., 2022. Mesenchymal stromal cell-derived septoclasts resorb cartilage during developmental ossification and fracture healing. Nat Commun 13, 571. https://doi.org/10.1038/s41467-022-28142-w

Storer, M.A., Mahmud, N., Karamboulas, K., Borrett, M.J., Yuzwa, S.A., Gont, A., Androschuk, A., Sefton, M.V., Kaplan, D.R., Miller, F.D., 2020. Acquisition of a Unique Mesenchymal Precursor-like Blastema State Underlies Successful Adult Mammalian Digit Tip Regeneration. Developmental Cell 52, 509-524.e9. https://doi.org/10.1016/j.devcel.2019.12.004

Stuart, T., Butler, A., Hoffman, P., Hafemeister, C., Papalexi, E., Mauck, W.M., Hao, Y., Stoeckius, M., Smibert, P., Satija, R., 2019. Comprehensive Integration of Single-Cell Data. Cell 177, 1888-1902.e21. https://doi.org/10.1016/j.cell.2019.05.031

van den Brink, S.C., Sage, F., Vértesy, Á., Spanjaard, B., Peterson-Maduro, J., Baron, C.S., Robin, C., van Oudenaarden, A., 2017. Single-cell sequencing reveals dissociation-induced gene expression in tissue subpopulations. Nat Methods 14, 935–936. https://doi.org/10.1038/nmeth.4437